Multilayer adsorption of deuterium hydride on graphite

Hong Wu* and G. B. Hess
Department of Physics, University of Virginia, Charlottesville, Virginia 22901
(Received 16 September 1997)

We report ellipsometric-coverage vapor-pressure isotherm measurements for HD on graphite over the temperature range 8.5–16.7 K. As many as 17 discrete layer adsorption steps are resolved at temperatures near 16.0 K, slightly below the bulk triple point ($T_t = 16.60$ K). Layer condensation critical temperatures are determined for layers two through nine. The sequence of critical temperatures indicates that the roughening temperature T_r of the close-packed facet of HD is certainly above 14.9 K and could be as high as T_t. With some assumptions, an estimate of $T_r = 15.3$ K is obtained. A conspicuous feature of the isotherms is occurrence of hysteresis and splitting over limited temperature ranges in the fourth, fifth, and sixth layer adsorption/desorption steps. This apparently indicates a change in structure of the underlying film when the thickness equals or exceeds four layers. [S0163-1829(98)00711-5]

I. INTRODUCTION

For certain combinations of adsorbate and substrate, films many layers thick grow in equilibrium with vapor as the pressure is increased towards saturation. Hydrogen on graphite is one such combination. Thus it is a system in which one can hope to study phenomena relating to growth from a quasi-two-dimensional (2D) monolayer toward a 3D crystal.

Several issues can be addressed in such a system. The first is to what extent complete wetting (uniform equilibrium film growth to macroscopic thickness) is approached. Wetting is favored by an attractive substrate-adsorbate potential that is stronger than the attractive potential between adsorbate molecules. If the film is solid, however, a strong substrate will induce strains in the film. At a sufficiently large thickness the positive strain energy will exceed the negative potential energy of interaction with the substrate, and the film will prefer not to be attached to the substrate: Wetting then should be incomplete.[1,2]

At low temperatures a solid film should grow layer by layer, through a series of first-order layer condensation transitions.[3,4] This means, for an ideal substrate, the coverage of the adsorbate in the film increases abruptly by about one molecular layer at particular values of pressure of the ambient vapor. If the temperature is raised, the first-order phase transition of nth layer condensation may terminate at a layer critical temperature $T_{c,n}$, beyond which the step in coverage no longer is vertical and rapidly broadens; film growth becomes continuous. As the layer number increases, $T_{c,n}$ should approach the roughening temperature T_R of the corresponding facet of the 3D crystal.[5,6] The relation of T_R to the bulk melting point T_t is of interest.[7]

More complicated behavior occurs in some cases. Argon, krypton, and xenon films on graphite show reentrant layering: In a temperature interval slightly above the apparent layer critical temperatures, sharp condensation steps reappear for the fourth and higher layers, shifted by about a half layer in coverage and chemical potential.[7–11] This is associated with disordering of the top layer and its interaction with the rest of the film.[12–14] Phillips, Zhang, and Larese[12] have attributed it to outer-layer melting driven by layer promotion, while other authors[13,14] have identified it with the preroughening transition that occurs in solid-on-solid lattice models.[15] Argon and nitrogen on boron nitride show similar behavior at least up to four-layer films,[16] indicating that the phenomenon is not highly sensitive to the strength of the substrate interaction. Other systems including Ne, N_2, and CO on graphite[17] have some features that are similar.

Other structural phenomena observed in different physisorption systems might possibly occur in hydrogen films on graphite: Neutron-diffraction study of three- and four-layer argon films[18] and x-ray-diffraction study of xenon trilayers[19] indicate that stacking faults are common. In solid hydrogens the difference in free energy between hcp and fcc structures is very small,[20] and there are indications that surface interactions can favor the metastable fcc structure.[21–24] Simulations for multilayer argon and methane on graphite suggest that the bottom layer can become incommensurate with the rest of the film due to substrate-induced lateral compression, and this is supported to some extent by neutron-scattering experiments.[25]

The adsorbates mentioned differ in interaction strength and the importance of quantum effects, but all are effectively spherical molecules: the rare gases intrinsically, methane due to rotation at the relevant temperatures, and hydrogen because in equilibrium at low temperatures the molecules are predominately in the $J = 0$ rotational state, little perturbed by the surface interactions.

In recent years, films of molecular hydrogen (H_2), deuterium hydride (HD), and molecular deuterium (D_2) on graphite, MgO, or BN substrates have been studied by volumetric vapor pressure isotherms,[26–30] heat capacity,[26,29,31] neutron diffraction,[31] low-energy electron diffraction,[32] nuclear magnetic resonance,[33] and elastic[28] and quasielastic neutron-scattering[34,35] (QENS) measurements. The volumetric isotherm study of H_2 on MgO by Ma, Kingsbury, Liu, and Vilches[26] showed layer-by-layer growth up to six or seven layers. Recently, Vilches and co-workers[29,36] have reported volumetric, heat capacity, and QENS measurements for bilayer HD on graphite, with the volumetric measurements extending up to four layers.

We have made ellipsometric isotherm measurements on

all three isotopic combinations, and report here the results for HD. Compared to H_2 and D_2, HD has the simplifying characteristic that it does not have a metastable ortho or para species, so possible effects of $J=1$ molecules and uncertainty in their concentration are not present. First we review briefly past work on multilayer HD. Vilches, Liu, Ebey, and Liu[29] made vapor pressure and heat-capacity measurements of bilayer HD on graphite. They found a conventional phase diagram for the second layer with a two-dimensional triple point (at 8.44 K) and critical point (about 11.45 K from heat capacity, 11.8 K from vapor pressure isotherms) corresponding, respectively, to solid-liquid-vapor coexistence and the limit of liquid-vapor coexistence. Liu[36] extended the isotherm measurements to the third and fourth layers, finding $T_{c,3}=12.3\pm0.2$ K and $T_{c,4}=12.0\pm0.2$ K. Vilches *et al.*[28] also made volumetric measurements of HD on MgO up to four-layer thickness; critical temperatures for the second, third, and fourth layers were determined to be 10.5, 12.1, and 12.4 K, respectively, close to the values on graphite above the second layer. The third and fourth layers did not show evidence of melting below the critical temperature or a liquid-vapor coexistence region. This is also true on graphite, but second-layer melting is much weaker on graphite,[36] so melting of higher layers could have been difficult to see in isotherms. Mobility studies of multilayer HD on MgO by QENS (Refs. 33 and 34) show that a liquidlike submonolayer on the surface persists below 8 K. The thickness of this quasiliquid layer grows to slightly less than 1 molecular layer (ML) at 12 K and at least 6 ML very near T_t. On graphite the mobile fraction in bilayer HD is very small below $T_{c,2}$ but there are no data for thicker films.[36]

II. EXPERIMENTAL APPARATUS AND PROCEDURE

Our adsorption cell is located within a cryostat, so that the cold walls of the cell and connecting tubing protect the graphite substrate from contamination resulting from outgassing of room-temperature walls or condensible impurities in the supply gas. The substrate, a $10\times5\times0.3\,\mathrm{mm}^3$ slab of highly oriented pyrolytic graphite (HOPG),[37] is clamped to a copper cold finger (the ''sample mount'') that is temperature regulated using a silicon diode thermometer and Lake Shore Cryotronics controller. A second copper cold finger is used to regulate the adsorbate vapor pressure inside the cell. The cell, sample mount, and cold finger are cooled by a Joule-Thomson third stage of a closed-cycle helium refrigerator. Manually adjusted heaters control the temperature of the body of the cell and the cold finger. The pressure in the cell is measured by three capacitance diaphragm gauges at room temperature, with ranges of 10, 100, and 1000 Torr. Raw pressure data are corrected for the thermomolecular effect using the equation of Takaishi and Sensui.[38]

We monitor the coverage of adsorbate on the graphite substrate by an ellipsometric technique: A suitably polarized light beam is reflected from the graphite sample at 45° angle of incidence, and analysis of the reflected light gives the ratio ρ of the reflection coefficients for p- and s-polarized light and the relative phase delay Δ between the two polarizations. If a transparent film is deposited on the reflecting surface, the principal effect is to increase the relative phase delay Δ by an amount proportional to the film thickness,

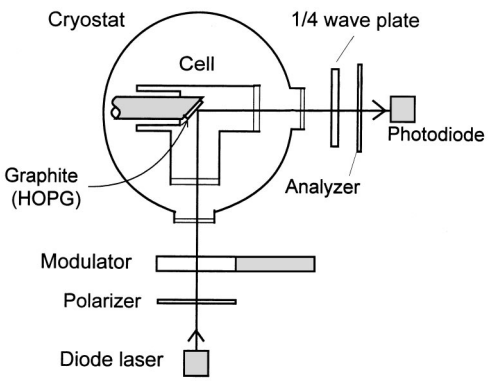

FIG. 1. Schematic diagram of the cell and optical setup, which is configured as a phase-modulated reflectance ellipsometer.

provided the film is very thin compared to the wavelength of the light. Details of our ellipsometric technique have been described previously.[39] Figure 1 shows the optical setup of the system. Light (at $\lambda=670$ nm) from a diode laser, which is linearly polarized at an angle of 45° to the plane of incidence, passes through a phase-delay modulator and reflects from the sample. The modulator, which is a rectangular prism of fused silica driven at its extensional resonance frequency, adds a 50-kHz ac phase delay to the sample phase delay Δ. The reflected light passes through a quarter-wave plate and an analyzer oriented at 45° to the plane of incidence, then to a photocell. The output of interest (I_1) is the Fourier component of the photocurrent at the modulation frequency. This is proportional to $\sin\Delta$, hence to the film thickness on the graphite substrate, when the quarter-wave plate has been rotated to null I_1 for the bare substrate.[39] This measure of coverage, I_1, is monitored as the pressure of adsorbate gas in the cell is increased to the saturated vapor pressure p_0 and then reduced (usually) until the second layer is desorbed. The process was repeated on many isotherms at approximately 0.1 K temperature increments.

In contrast to the volumetric technique, these measurements do not use a large-area powder sample, and therefore are not limited by capillary condensation as p approaches p_0.

III. RESULTS

We conducted three experimental runs with HD, spanning the temperature range 8.5–16.7 K. The first run consisted of 140 isotherms and the second 99 isotherms. Prior to these two runs the substrate had extended exposure to air when we replaced the cell body and was cleaned by heating *in situ* under vacuum to 300 °C overnight. Figure 2(a) shows a selected isotherm at $T=11.75$ K in the second run. In addition to sharp steps, we see some broad features between steps, notably above the second and below the fourth step, which we attribute to adsorption on a contaminated fraction of the observed portion of the substrate surface. We then replaced the HOPG sample and repeated the original preparation procedure, cleaving in air with adhesive tape and baking in flowing argon at 500 °C. The sample was then installed in the cell and was heated *in situ* as before. The third run, in which 57 isotherms were obtained, was conducted with this sample. Figure 2(b) shows an isotherm also at $T=11.75$ K

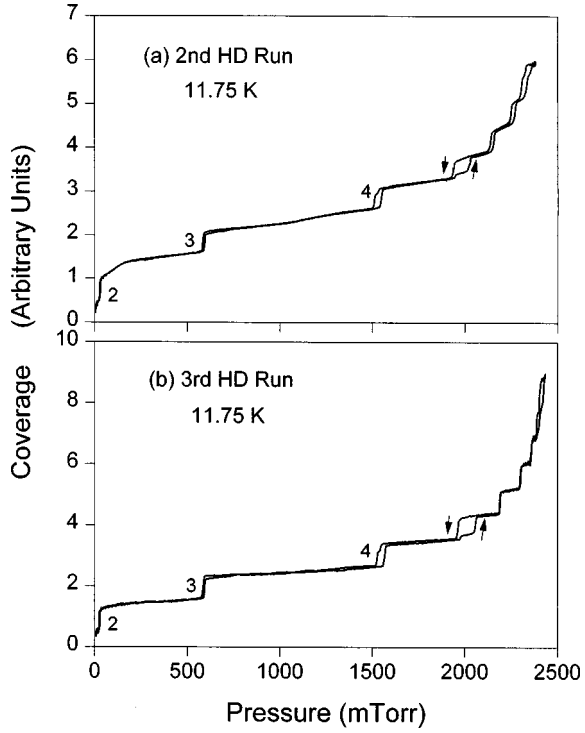

FIG. 2. Adsorption isotherms for HD on graphite at 11.75 K, shown as ellipsometric coverage vs pressure: (a) from the second run (partially contaminated substrate); (b) from the third run (clean substrate).

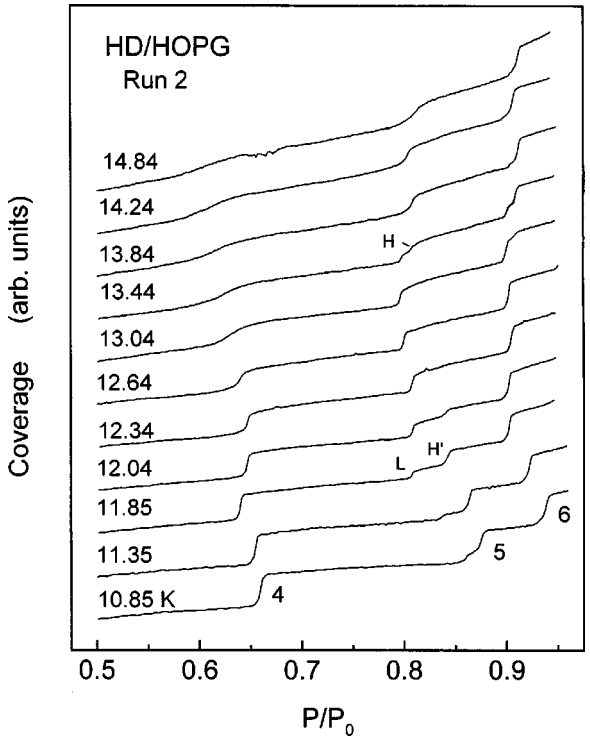

FIG. 3. Family of HD adsorption isotherms at selected temperatures, labeled on the left, from the second run. A range of reduced pressure including the fourth, fifth, and sixth steps is shown.

from this third run. It is similar to the earlier isotherm, but the individual steps are about 1.5 times as high (not apparent in the normalized figures) and the regions between steps are flatter. A close comparison of the two isotherms in Fig. 2 reveals that the risers, especially of the higher steps, on the contaminated substrate are less steep than on the clean substrate. For instance, the slope (dI_1/dp) of the sixth step in Fig. 2(a) is about half of the slope of the sixth step in Fig. 2(b). Even on a clean substrate in a first-order condensation region isotherm steps are not perfectly vertical, due to residual heterogeneity of the substrate and to finite size of substrate grains. Another difference is that the maximum number of layers observed at saturation on a contaminated substrate is less than on a clean substrate: We see 8.5 layers in Fig. 2(a), compared to 10.5 layers in Fig. 2(b). As is discussed later in this paper, substrate heating by the laser beam could affect the total film thickness, but in the present case both isotherms were measured at nearly the same laser power. In fact, we see two less layers in almost all isotherms in the second run compared to the third run. A possible explanation is given by the grain boundary model of Dash,[40] if the substrate in the second run had uniform patches of smaller average diameter.

In the two isotherms of Fig. 2 there is nearly identical splitting and hysteresis in the fourth and fifth steps. The splitting of the fourth step was observed only on the descending branch, which corresponds to layer evaporation from the substrate. Splitting of the fifth step and also the sixth step (not seen in Fig. 2, but in higher temperature isotherms) was observed only on the ascending branch, which corresponds to layer condensation on the substrate.

From these observations and similar comparisons with the other isotherms of the third run, we conclude that in the first two runs part (about one-third) of the substrate surface was covered by a tightly bound layer of an unknown contaminant. The remaining part, though slightly degraded, perhaps by point impurities or reduced patch size, was essentially clean graphite. We therefore interpret the sharp features in these runs as characteristic of HD on graphite (of slightly reduced quality) and use them in the analysis which follows. In Fig. 3 we show portions of selected isotherms for adsorption from the second run, for the range of reduced pressures 0.5–0.95. This provides an overview of the fourth-layer critical point and step splitting in the fifth and sixth layers

We first analyze the layering behavior, measuring the pressure at each step and the slope of the step riser at its inflection point. From these slopes we calculate step widths in chemical potential using $\Delta\mu = T\Delta p/p$. The pressure width Δp is obtained by dividing a nominal step height ΔI_1 by the measured slope (dI_1/dp) at the inflection point. Figure 4 shows the condensation step widths for steps two to four. Below ~ 12 K the transitions are apparently first order, with widths determined by substrate heterogeneity or, at the lowest temperatures, by film growth kinetics. Each step broadens at higher temperatures. This is interpreted as passage through a critical point into the hypercritical region. From plots of step width against temperature we estimate the layer critical temperatures to be $T_{c,2} = 11.4 \pm 0.2$ K, $T_{c,3} = 12.1 \pm 0.2$ K, and $T_{c,4} = 12.3 \pm 0.2$ K. In this analysis, we assume that the compressibility along the critical isochore above the critical temperature T_c varies as $(T - T_c)^{-\gamma}$, with $\gamma = \frac{7}{4}$, the value for the 2D Ising model. These layer critical temperatures are consistent with the values obtained by Vilches and co-workers,[28,36] cited above.

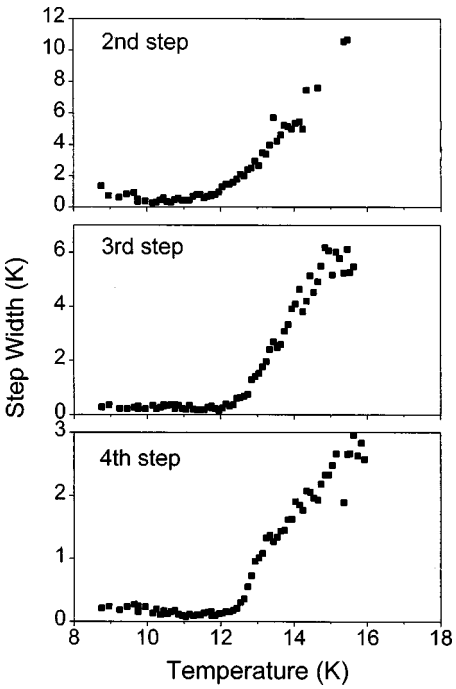

FIG. 4. Widths of the second-, third-, and fourth-layer condensation steps as functions of temperature. Note that the fourth step width above the critical temperature has an inflection point near 13 K and cannot be fit over more than a limited range by the $\frac{7}{4}$ power law that is expected in the critical region of an Ising transition.

In certain temperature ranges we see hysteresis accompanied by splitting in the fifth- and sixth-layer condensation steps and in the fourth-layer evaporation step, as discussed above. These occur in the range 9.45–12.34 K for the fourth step, 10.85–12.34 K for the fifth step, and again at 12.64–14.84 K for both the fifth and sixth steps. Figure 5 shows portions, including the fourth and fifth steps, of selected complete isotherms near 12 K, in both condensation and evaporation. One can see the evolution with temperature of the splitting and hysteresis. We remark that there could be apparent hysteresis due to a temperature shift between condensation and evaporation steps if the pressure were reduced too rapidly from saturation, because the sample temperature can be pulled down by evaporation of bulk adsorbate. But here this is not the case, as the pressure scans were sufficiently slow that the condensation and evaporation steps coincide for layers seven and eight. With increasing temperature, at 10.85 K we first see a small substep at the bottom of the fifth step. Though this substep becomes more pronounced, its height does not change much until 11.75 K; above this temperature the low-pressure part becomes taller and high-pressure part becomes correspondingly smaller as temperature increases. The maximum pressure offset between the low and high components is about 4%. By 12.34 K there is no longer a distinct upper substep, leaving just the low-pressure part. We label the bottom substep (low-pressure part) as L and the top part as H'. Figure 5 shows the evolution of step 5 from predominantly H' to predominantly L on increasing temperature. Concurrently, the hysteresis associated with the lower substep becomes smaller as temperature increases from 10.85 to 12.34 K. The fourth step splits almost antisymmetrically to the fifth step: Splitting starts from the top of the desorption step instead of from the bottom of the condensation step, but maintains about the same fractional height. One possible interpretation would be that at any fixed temperature there is a distinct portion of the substrate that is contributing the low substep of fifth-layer condensation and the high substep of fourth-layer evaporation, i.e., this portion avoids the hysteresis that occurs on the rest of the substrate. With increasing temperature the less-hysteretic behavior expands to the whole substrate.

Over the higher temperature range, 12.64–14.84 K, we observe splitting and hysteresis in the fifth and sixth steps. Figure 6 shows portions of selected complete isotherms go-

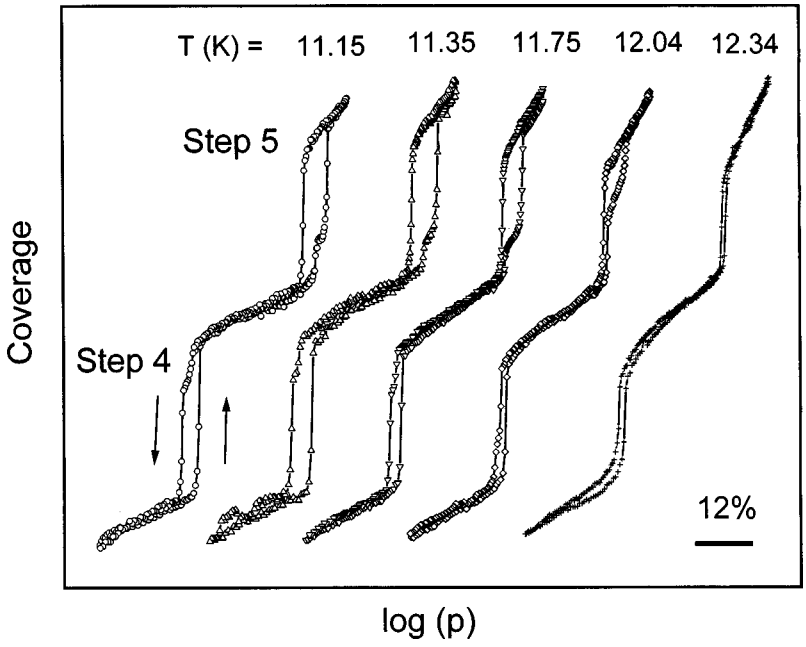

FIG. 5. Portions corresponding to the fourth and fifth steps from complete adsorption and desorption isotherms. Temperatures are given at the top. The abscissa is logarithm of pressure, with arbitrary offsets; the bar indicates the scale. The ordinate is coverage, in arbitrary units.

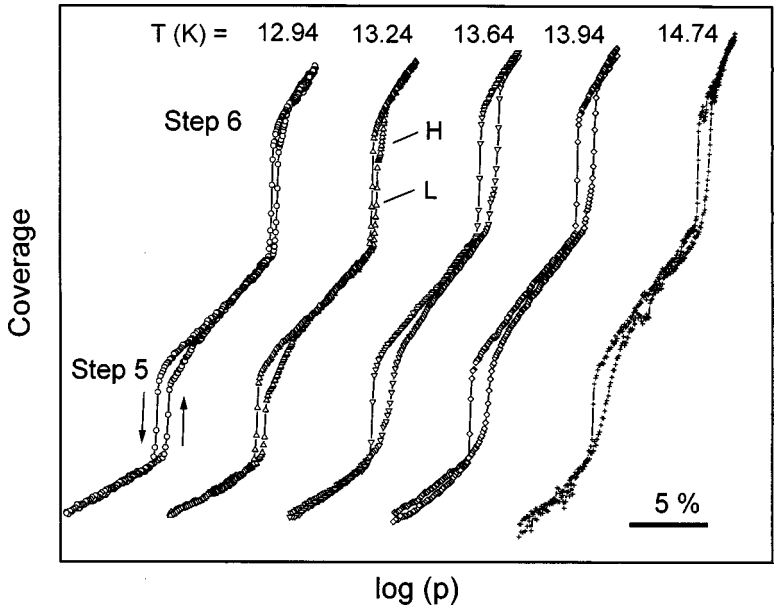

FIG. 6. Portions corresponding to the fifth and sixth steps from complete adsorption and desorption isotherms at several higher temperatures.

ing both up and down. Below 12.64 K we see an unsplit sixth step. The top part of the step is rounded at 12.84 K and develops into a separate substep by 13.04 K. If we label the bottom part still as L and the top part as H, Fig. 6 shows that the height of substep H increases while L decreases with increasing temperature. From 13.84 K to 14.64 K, the height of L is small and changes only slowly, and we still can see a small low-pressure part until 14.84 K. Above this temperature, only the high-pressure part remains. Thus by the appearance and evolution of the substep, the sixth step evolves from L to H character, and thus from less to more hysteretic. The maximum pressure offset between the low and high substeps is about 1%. We find very similar splitting and hysteresis in the fifth step over the same temperature range, as is shown in the lower part of Fig. 6.

The fifth- and sixth-layer desorption steps are sharper than the condensation steps for temperatures above 13.5 K. This is shown more clearly in Fig. 7, where we plot the widths of both the fifth-layer adsorption (up) and desorption (down) steps, as well as the sixth-layer condensation step, against temperature. We further observe that the sharpness of the fifth- and sixth-layer condensation steps is history dependent, i.e., depends on how low the pressure is taken in the course of ramping down and then up. The sharpness of the fifth- and sixth-layer evaporation steps is not affected by the history. If we go below the second step (as is the case in Fig. 6), we see broader fifth- and sixth-layer condensation steps compared to their corresponding evaporation steps. If we do not desorb the fourth layer before reversing, as is the case in Fig. 8, we see sharp fifth- and sixth-layer condensation steps that have almost the same slopes as the corresponding evaporation steps, and the hysteresis loop is narrow. This suggests that memory of the trilayer structure is responsible for most of the hysteresis seen in complete isotherms in steps five and six.

In Fig. 7 the width of each substep is still defined in terms of a nominal *full* step height. We use different symbols, squares for low-pressure part, triangles and crosses for high-pressure part. Step six undergoes only one transition, from low-pressure to high-pressure part, with increasing temperature. Step five undergoes two transitions, from high-pressure to low-pressure part near 12 K and from low pressure back to high-pressure part near 13.5 K. There is no reason to believe

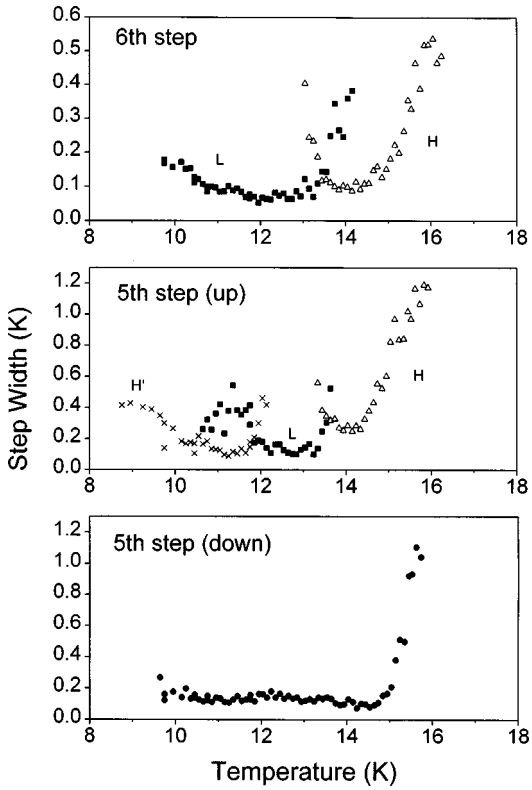

FIG. 7. Widths of the fifth-layer adsorption (up) and desorption (down) step and width of the sixth-layer adsorption step as functions of temperature. For adsorption, squares represent low-pressure part L and triangles represent high-pressure part H. Crosses represent another high-pressure part H' for the fifth step at low temperatures.

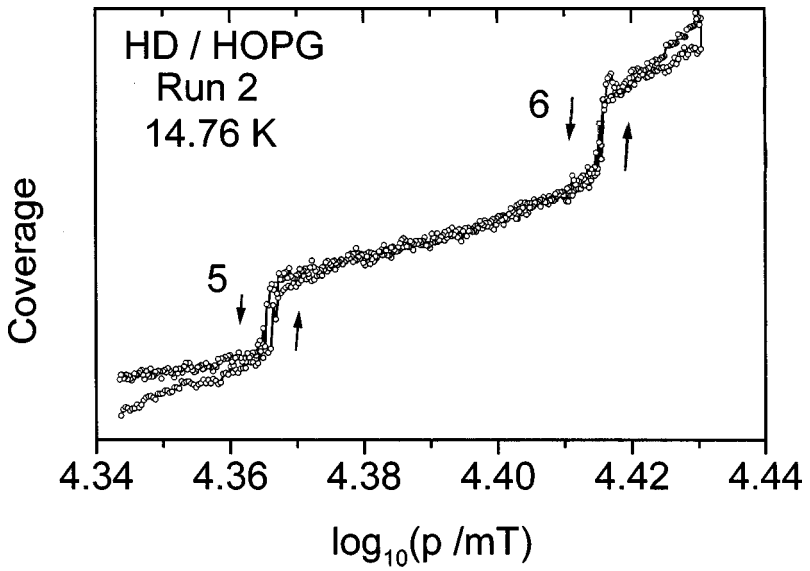

FIG. 8. Portion corresponding to the fifth and sixth steps of an adsorption and desorption isotherm at 14.76 K. In this case, the adsorption branch immediately followed reduction of the pressure from saturation, so that the film thickness did not go below four layers.

the two high-pressure parts correspond to the same structure, so we label one H', the other H. From the data in Fig. 7 we have attempted to obtain the critical temperatures that bound (possibly) first-order regions. For step six there are two such temperatures: 13.3 K terminating the L first-order region, and 14.7 K terminating the H first-order region. For fifth-layer condensation there are three such temperatures: 11.7 K terminating the H' first-order region, 13.3 K terminating the L first-order region, and 14.2 K terminating the H narrow-step region. *Desorption* isotherms give $T_{c,5}=14.7\pm0.1$ K and $T_{c,6}=14.85\pm0.1$ K. On the basis of our earlier discussion, these should be characteristic of the equilibrium structure. The widths of layer condensation steps seven through nine are shown in Fig. 9. There is little hysteresis in these steps. We find layer critical temperatures: $T_{c,7}=14.8\pm0.1$ K, $T_{c,8}=14.95\pm0.2$ K, and $T_{c,9}=14.8\pm0.1$ K. In addition, there is a systematic uncertainty in the temperature scale of ±0.2 K. It is expected that these critical points near 15 K are related to roughening of the close-packed facet of bulk HD; this is discussed below.

Thermodynamic information about the adsorbate can be presented as chemical potentials of layer coexistence. From the vapor pressure p_n at condensation of the nth layer, we calculate the chemical potential μ_n at the coexistence of n and $n-1$ layers, relative to that of bulk solid-vapor coexistence, using the equation

$$\mu_n-\mu_0=T\ \ln(p_n/p_0). \tag{1}$$

(We set $k_B=1$.) Chemical potentials for layer condensation steps two through eight are plotted in Fig. 10, using data from the second HD run. Figure 11 is an expanded plot for layers four to nine. For the fifth- and sixth-layer substeps we use the same symbols as in the step-width plots. All layer chemical potentials have negative slopes. There seem to be two changes in slope in several of the higher layer condensation lines, one near 12 K and the other near 14 K.

Heating of the graphite substrate by the laser beam (150–650 μW outside the cryostat entrance window) could contribute to the negative slopes at lower temperatures. In the first HD run, we first made isotherm measurements at temperature increments of 0.2 K with a laser power of 120 μW, then we filled in the intervening temperatures at a laser power of 260 μW. We found that below 12 K, the chemical potentials measured at higher laser power have larger negative slopes, while above 12 K the two sets of chemical potentials fall on the same line. We made a more detailed study of laser heating in an earlier experiment with neon on

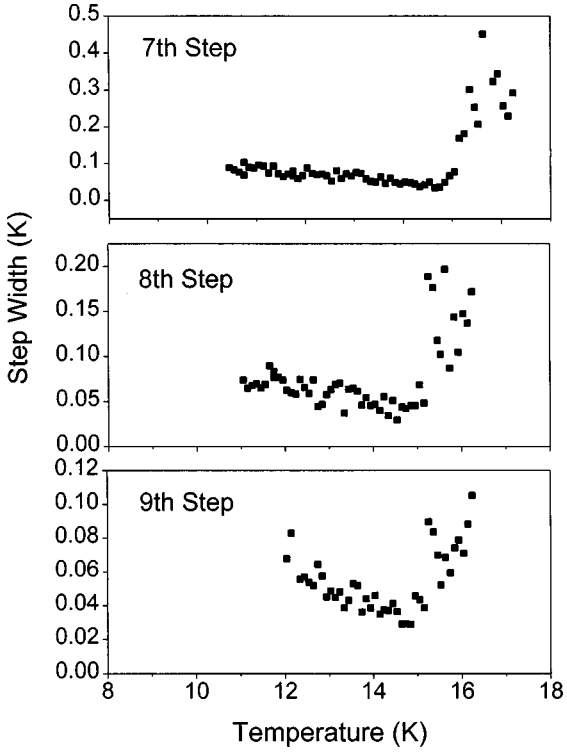

FIG. 9. Widths of the seventh-, eighth-, and ninth-layer condensation steps as functions of temperature. The background widths are attributed to the effect of substrate heterogeneity or, at lower temperatures, film growth kinetics.

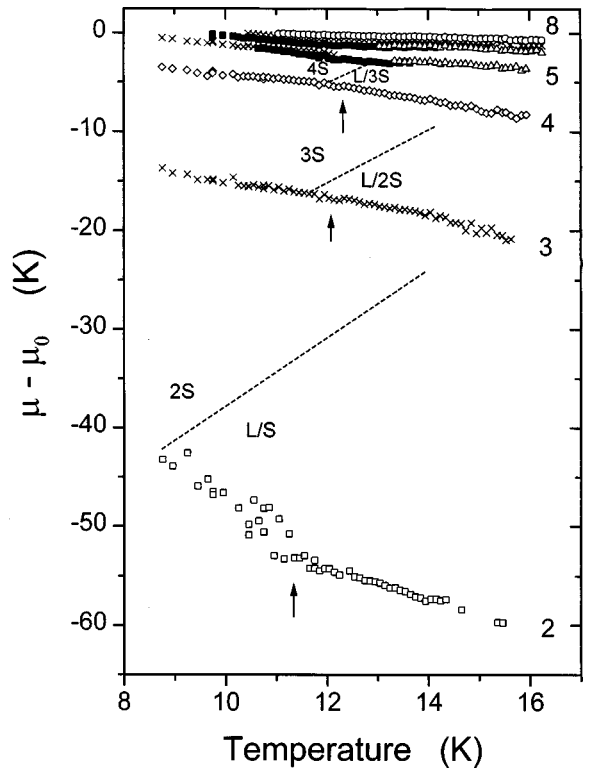

FIG. 10. Chemical potential (relative to bulk solid-vapor coexistence) at condensation of layers two through eight, as functions of temperature. Layers are labeled at the right. For the fifth and sixth steps, solid squares represent the low-pressure substep, open triangles represent the high-pressure substep (observed at higher temperatures), and crosses represent the high-pressure part of the fifth step at low temperatures. Dashed lines indicate the melting line of the second layer (from Ref. 36) and conjectured melting lines of the third and fourth layers. Labels of the form ''$nL/n'S$'' indicate the approximate structure in terms of the numbers of liquid and solid layers. The arrows indicate layer critical points.

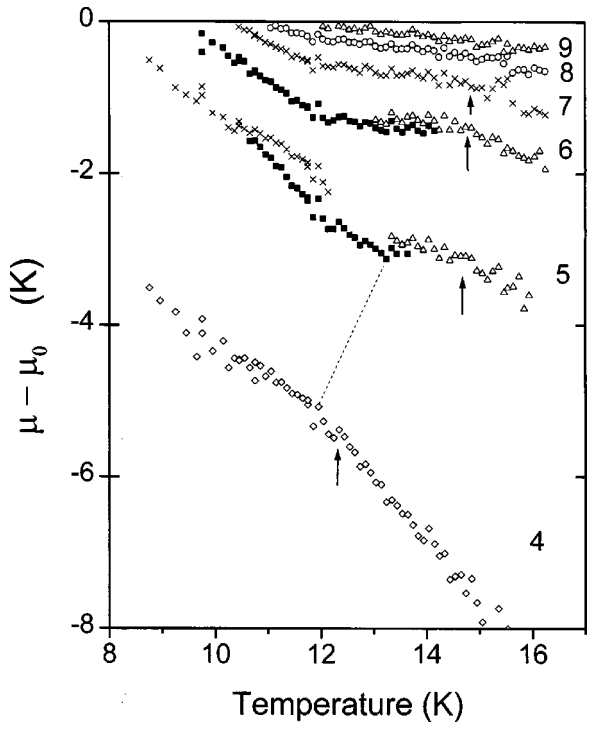

FIG. 11. Expansion of the chemical-potential temperature diagram in the region of layers four through nine. The symbols are the same as in Fig. 10. The dashed line is a conjectured melting line of the fourth layer, based in part on the changes in slope of the layer condensation lines. The arrows indicate layer critical points.

graphite[17] and found that laser heating had little effect when the pressure in the adsorption cell was above about 1 Torr. From the observations in the first HD run and the neon experiment, we believe that the upward curvature of the layer chemical potentials in Fig. 10 below 12 K, and especially below 10 K, is very likely due to heating by the laser beam. Above 12 K, layers above the second (with step pressures close to 1 Torr or higher) probably are not much affected by laser heating. For the second layer, laser heating may persist to temperatures slightly higher than 12 K, since at 12.06 K the second step pressure is still low, about 36 mTorr. Thus we believe that the negative slopes above 12 K (except the second layer) represent the intrinsic properties of the HD film. The changes of slope above 14 K should be affected even less by laser heating and reflect increased partial entropy of the film, which we analyze next.

Information about entropy of added layers can be obtained from the μ-T phase diagram by use of the Maxwell relation

$$(\partial S/\partial N)_T = -(\partial \mu/\partial T)_N , \tag{2}$$

where N is the number of molecules of adsorbate per unit area of substrate and S is the entropy of the adsorbate per unit area. Applied to a coverage in the coexistence region of n and $n-1$ layers, the right side of this equation is the negative slope of the coexistence line in the μ-T phase diagram and the left side is the partial entropy on adding to the nth layer. Above the layer critical temperature, the locus of broadened nth layer steps will still correspond approximately to a line of constant N. Since we plot μ relative to the chemical potential of bulk solid, the partial entropy is relative to the entropy of bulk solid. In the temperature range 12–14 K, the negative slopes of layer chemical potentials in Figs. 10 and 11 decrease with layer number from 1.72 for the second layer to 0.93 for the third, 0.83 for the fourth, 0.18 for the fifth, and approaching zero for the higher layers. This implies that the partial entropy (in units of k_B) for each layer is larger than the entropy of bulk solid by these amounts. For comparison, the entropy difference between bulk liquid and solid HD is 1.15 k_B at the triple point. These entropies imply that condensation of the second, third, and fourth layers is adding disordered material to the film, which is consistent with the temperature range being above the critical temperatures of these layers, while condensation of the fifth and higher layers is adding material (nearly) as ordered as solid. (The added solid layer may be under a disordered surface layer, which is displaced outwards.) Although not seen in our experiment, there are presumably layer solidification lines sloping upward between the layer condensation lines in Fig. 10. For HD, the second-layer solidification line has been observed in volumetric isotherms,[36] extending from a triple point at 8.44 K to a point still well below the third layer at 13.28 K. This transition is indicated by a dashed line in Fig. 10. In the case of D_2/graphite, layer melting transitions are seen in heat-

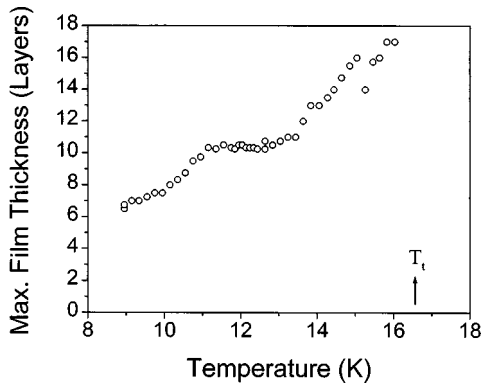

FIG. 12. Maximum HD film thickness which can be resolved as layer by layer growth (i.e., steps in isotherms), as a function of temperature. These data are from the third run.

capacity scans up to the fourth layer[31] and originate at triple points less than 1 K below the corresponding layer critical temperatures. Conjectured melting lines for the top layer of three- and four-layer HD films are indicated by additional dashed lines in Figs. 10 and 11. The calorimetric molar entropy change associated with the melting line in second-layer HD/graphite is only 0.073 k_B, indicating that disordering of the quasiliquid layer develops over an extended temperature range.

The limiting film thickness on approach to saturation is finite, for reasons that may be partly technical and partly intrinsic to the interaction of HD with graphite. Isotherms show distinct (although not vertical) layer steps up to saturation at temperatures up to 16.04 K. The maximum HD film thickness is shown in Fig. 12 as a function of temperature from 8.96 to 16.04 K, using data from the third HD run (our best substrate). At temperatures between 15 and 16 K, we see about 16 or 17 layers. At lower temperatures the maximum thickness decreases, then reaches a plateau of 10 to 11 layers between 13.44 and 11.15 K. At still lower temperatures it decreases to about 6 layers at 9 K. As discussed earlier, laser heating has observable effects at temperatures below 12 K for HD on graphite. When we reduced the laser power from 630 to 120 μW at 10.46 K, we saw one more higher step. A temperature difference between the sample mount and the graphite substrate might be caused also by heat flux through the vapor from the slightly warmer cell walls, although partially shunted by the copper cap. Thus, the decreasing maximum thickness with decreasing temperature below 11 K in Fig. 11 could be due to laser heating and may not be intrinsic.

Above 16.04 K growth is continuous instead of stepwise. (Note that this is well above the critical temperatures of the eighth and ninth layers, although it still may be near or below the roughening temperature.) However, the maximum ellipsometric signal does not increase significantly up to the triple point. At 16.74 K (0.14 K above the triple point, not shown in Fig. 12) the film has grown to a thickness equivalent to about 31 layers. This suggests triple-point wetting of HD on graphite due to release of stress when the film becomes liquid.[2,40,41] It is also further evidence that the limiting thickness of the solid film at intermediate temperatures is not due primarily to a temperature gradient.

IV. DISCUSSION

Wetting. Near 16 K we have observed thicker layered solid films than have been seen in other systems;[7] nevertheless the thickness is apparently limited by strain.[2,40,41] The increase in limiting thickness above 13 K may be due in part to surface melting, which relieves strain in the quasiliquid portion of the film. Neutron diffraction data for H_2 and D_2 indicate that the completed monolayer has 9–14 % greater density than the (111) plane of bulk solid.[31] Bilayer and trilayer D_2 films at low temperature have a mutually commensurate oblique structure, considerably distorted from equilateral, presumably to accommodate the resulting stress.[31,32] Similar structure is seen for H_2, although it appears only at the beginning of the succeeding layer; it is therefore probable that HD has the same structure. Trilayer data for D_2 have been interpreted as indicating *ABC* stacking.[42] If these conclusions are true for HD, then the trilayer differs from the bulk hcp structure both in stacking sequence and more important in distortion from threefold rotational symmetry, and some sort of structural change must occur on growth beyond three layers. Although the entire film could revert to the bulk hcp structure on further growth, this would incur increased interfacial energy at the substrate boundary. Alternatively, at some thickness, loss of registry could occur between different structures in the bottom layer (or two) and the rest of the film, to partially relieve the strain.[43] We discuss this more specifically below.

Layer critical temperatures. Critical temperatures, above which growth is continuous, are estimated above for layers two through nine. For layers two, three, and four these critical temperatures are in the vicinity of 12 K, but from layer five on they move to just below 15 K and then increase very slowly. It is apparent from the highest isotherm in Fig. 6, and also in Fig. 8, that the fifth layer remains sharp in *desorption* above the apparent critical temperature determined from the adsorption data. As the desorption data presumably represent the thick-film structure, these are the appropriate data to use in estimating the roughening temperature. The same is true of the sixth layer. This is confirmed by isotherms which cycled only between four complete layers and saturation, as in Fig. 8: Adsorption is then nearly identical to desorption. Therefore, we have used desorption data in determining T_{c5} and T_{c6}; for higher layers there is little hysteresis, and adsorption data were used.

The sequence of critical temperatures is expected to approach the roughening temperature of the close-packed HD face asymptotically as[5,6]

$$T_R - T_{c,n} \sim A/[\ln(n) - B]^2, \tag{3}$$

where A is an unknown nonuniversal constant and B is related to parameters that are imprecisely known. Due to the weak logarithmic dependence on n, the roughening temperature may be significantly above the highest layer critical point observed.[5,6] Even if layer five is assumed to be in the asymptotic region, given the scatter of our experimental data, and with two unknown parameters in addition to T_R in Eq. (3), it is not possible to conclude more than that $T_R \geqslant 14.9$ K. Indeed, even if data were available extending to much thicker films with an order of magnitude less scatter, T_R still would not be closely constrained unless either A or B

were fixed independently. B can be estimated theoretically, using the universal value for the surface stiffness at the roughening temperature, as $B \approx -1.9 + \ln(g)$, where g is a constant of order unity.[44] A fit with the fixed value $B = -1.9$ gives $T_R = 15.3 \pm 0.1 \pm 0.2$, where the second error is the systematic uncertainty in our thermometer calibration. This interpretation may be oversimplified. It is apparent in Fig. 9 that steps seven, eight, and nine do not continue to broaden rapidly above 15.3 K, and in fact steps eight through eleven remain conspicuous in the isotherms up to about 16.2 K.

Layer chemical potentials. The measured layer chemical potentials can be compared quantitatively to a simple theoretical model. The simplest assumption about the film structure is the Frankel-Halsey-Hill (FHH) model, as described by Steele:[45] The basic assumption is that the film is equivalent to a slab of bulk adsorbate placed in the attractive field of the substrate with no relaxation. In this case the chemical potentials are given approximately by[46]

$$\mu_0 - \mu_n - C_3/d^3(n-\tfrac{1}{2})^3, \tag{4}$$

where C_3 is the difference between the van der Waals coefficients of the substrate and the adsorbate and d is the HD layer spacing. Of the available data, those for films of five and more layers in the neighborhood of 13 K may come closest to satisfying the basic assumption: The layer transition lines are nearly horizontal, implying that the partial entropies are close to the entropy of bulk solid HD. Equation (4) gives a reasonable fit to these data with $C_3/d^3 = 310$ K and an offset of 0.4 K. This coefficient is about 50% larger than expected using C_3 from Vidali *et al.*[47] and $d = 3.03$ Å.[20] The offset reflects the energy contribution (e.g., strain), which is preventing complete wetting. The rather poor agreement on C_3 may indicate that the FHH approximation is not adequate, at least for layers as low as the fifth or sixth.

Hysteresis and step splitting. The most unexpected feature of our results is the hysteresis and step splitting described earlier. The occurrence of significant hysteresis only in certain layering transitions and only over limited temperature ranges is evidence that structural changes are occurring that are nucleated less easily than simple layer condensation. Splitting of steps at a temperature-dependent fraction of a layer suggests that the underlying film is different on different patches of the surface, or at least the nucleation barrier for the next layer is different. The sharpness of the substeps (at some temperatures) implies that these patches are not microscopic. Stable and metastable underlayer film structures may be present simultaneously on different graphite grains. One possibility for the process occurring at a split step is that the final states of the substeps are the same, but there are different nucleation barriers from the different initial states. Another possibility is that one substep represents growth of the equilibrium structure, the other continued growth of a metastable structure, and the difference persists in the thicker film. The latter might account for the similar splitting of layers five and six over the range 13–14 K.

A third possibility is that the steps are split in equilibrium. One explicit model in which this occurs is the ''intermeshing'' phase diagram of Weichman and Prasad,[48] for which *both* flat and disordered-flat surfaces are stable over a finite temperature interval. However, if the split steps on adsorption represent equilibrium, metastable states would have to be involved on desorption, and it is unlikely that such a model is the explanation for the present results.

Ordinarily the desorption step corresponds more nearly to the equilibrium layering transition than the adsorption step.[49] This is because grain edges are nuclei for desorption, but adding a layer may require overcoming a nucleation barrier. This is supported by the observation that the desorption steps are generally steeper. This may not be true if desorption is accompanied by a change in the equilibrium structure of the remaining film, as is apparently the case here in desorption of the fourth layer below 12 K.

In order to frame a conjecture on the origin of the splitting, we start by reviewing the behavior at a slightly lower temperature, 9 K. This is well below the layer critical temperatures, so layer condensation steps should be vertical except for kinetic effects. However, the vapor pressure is high enough to allow considerable precision. At 9 K there is no splitting. The second and third steps are sharp both in adsorption and desorption. (This is seen most clearly in isotherms of the third run.) No hysteresis is resolved in the second step; the hysteresis $\delta p/p$ is 5% in the third-layer step. The fourth step is unusual in being sharp in adsorption but broad in desorption, with hysteresis of about 6%. The fifth and sixth steps are broad in adsorption but sharp in desorption, with hysteresis of about 8%.

This suggests that structural changes involving a significant nucleation barrier occur on adding the fifth (and sixth) layer and on removing the fourth layer. As discussed above, there is reason to believe that the trilayer film has oblique structure considerably distorted from equilateral.[31] We conjecture that this structure is retained on (the sharp) adsorption of the fourth layer, but before or on adsorption of the fifth layer, the film seeks a different way to accommodate the stress at the graphite-HD interface. A likely possibility is a close-packed (hcp) structure for the outer part of the film, incommensurate with a more-dense monolayer or bilayer adjacent to the substrate. The broad sixth layer adsorption step indicates that some fraction of the metastable structure remains, or else further relaxation in the structure is occurring. The sharp sixth- and fifth-layer desorption steps suggest that the thick-film structure remains stable or metastable down to the four-layer film, but reverts to the oblique structure on removal of the fourth layer. We cannot say which is the stable structure for the four-layer film.

Above about 10.6 K, splitting of the fifth-layer adsorption step is observed, as apparently the fifth layer condenses at lower overpressure than before on a small but increasing fraction of the substrate. This presumably reflects an increasing nucleation probability for the lower-free-energy structure, perhaps dependent on grain size. Above 11.7 K the hysteresis associated with this lower substep has decreased to 1%. By 12.3 K the lower substep has grown to encompass the entire layer. Consequently, in the neighborhood of 12.5 K, the fifth-layer adsorption and desorption are both sharp, with little hysteresis. The same is true of the fourth and sixth layers (see Figs. 5 and 6). Thus equilibration of the structural change apparently occurs rapidly at this temperature on the whole substrate. An interesting possibility is that efficient relaxation to the equilibrium four-layer structure occurs when the fourth-layer solid grows from fourth-layer liquid

instead of from the vapor. There is no heat capacity data in this coverage range, but slopes in the chemical potential diagram (Fig. 11) suggest that the top layer of the four-layer film melts at about 12.0–12.3 K (in coexistence with layer three) to about 13 K (in coexistence with layer five). As the melting lines are not visible in the ellipsometric experiment, hysteresis there would not be observed.

What, then, accounts for the splitting of the fifth- and sixth-layer adsorption steps in the temperature range 13–14 K? We have suggested that the top layer of the compressed four-layer film is melted above about 13.2 K. The chemical potentials of fifth- and sixth-layer condensation remain quite flat over 13–14.2 K, suggesting that no additional melting (below the top layer) occurs in this temperature range. This is consistent with QENS data for HD on MgO, which indicate about one liquid layer on thick films at this temperature.[28,34,35] Melting of the top layer plausibly could cause reversion of the equilibrium four-layer film (now three solid layers) to an oblique structure and also produce close competition between structures in the five-layer film (four solid layers). Thus the process occurring at lower temperatures could be repeated one layer higher. There are two differences: The fourth-layer step at 11–12 K shows splitting on desorption, whereas the fifth-layer step near 13 K shows splitting on adsorption. This might be understood if the free energies are shifted to favor slightly more an oblique structure in the latter case. Second, in the lower temperature range the level of splitting in adsorption moves *up* (less of the film becomes hysteretic) with increasing temperature, whereas in the higher temperature range the level of splitting moves *down* (more of the film becomes hysteretic) with increasing temperature. This may be related to the first appearance of a quasiliquid layer in the four-layer film near 13 K and its increasing disorder with increasing temperature. This sequence does not continue because films of five and more layers have melting transitions only near their critical temperatures, which are near 15 K.

Additional experimental results from cycling the pressure up and down through a single step, or a few steps, can be examined in light of this picture. The general result is that hysteresis is reduced if the film thickness does not cycle below four layers. In repeated cycling through just the fourth-layer step below 12.5 K, we still observed splitting on the desorption side, but it occurred near the bottom of the step; thus 80–90 % of the film was remaining in the thin-film structure. On repeated cycling through the fifth step alone at temperatures near 10.4–12 K, we saw no splitting on adsorption but sometimes slight splitting on desorption, as in the fourth step. The former is consistent with remaining in the thick-film structure throughout the cycle, or making a rapid transition to it when the fifth layer is added.

ACKNOWLEDGMENTS

We thank Professor O. E. Vilches for helpful discussions and for communicating experimental results prior to publication, and W. F. Saam and E. Kolomeisky for communications relating to roughening. This work was supported by the National Science Foundation under Grant No. DMR-9320860.

*Present address: KCS Computer Services, Inc., 777 Penn Center Blvd., Pittsburgh, PA 15235.

[1] A. D. Migone, J. Krim, J. G. Dash, and J. Suzanne, Phys. Rev. B **31**, 7643 (1985).
[2] C. Ebner, C. Rottman, and M. Wortis, Phys. Rev. B **28**, 4186 (1983).
[3] M. J. de Oliveira and R. B. Griffith, Surf. Sci. **71**, 687 (1978).
[4] R. Pandit, M. Schick, and M. Wortis, Phys. Rev. B **26**, 5112 (1982).
[5] D. A. Huse, Phys. Rev. B **30**, 1371 (1984).
[6] M. P. Nightingale, W. F. Saam, and M. Schick, Phys. Rev. B **30**, 3830 (1984).
[7] G. B. Hess, in *Phase Transitions in Surface Films 2*, edited by H. Taub *et al.* (Plenum, New York, 1991), p. 357.
[8] H. S. Youn and G. B. Hess, Phys. Rev. Lett. **64**, 918 (1990).
[9] H. S. Youn, X. F. Meng, and G. B. Hess, Phys. Rev. B **48**, 14 556 (1993).
[10] P. Day, M. Lysek, M. LaMadrid, and D. Goodstein, Phys. Rev. B **47**, 10 716 (1993).
[11] P. Day, M. LaMadrid, M. Lysek, and D. Goodstein, Phys. Rev. B **47**, 7501 (1993).
[12] J. M. Phillips, Q. M. Zhang, and J. Z. Larese, Phys. Rev. Lett. **71**, 2971 (1993); Q. M. Zhang and J. Z. Larese, Phys. Rev. B **52**, 11 335 (1995).
[13] P. B. Weichman, P. Day, and D. Goodstein, Phys. Rev. Lett. **74**, 418 (1995).
[14] S. Prestipino, G. Santoro, and E. Tosatti, Phys. Rev. Lett. **75**, 4468 (1995); S. Prestipino and E. Tosatti, Surf. Sci. **377–378**, 509 (1997); See also D. L. Woodraska and J. A. Jaszczak, Phys. Rev. Lett. **78**, 258 (1997).
[15] M. den Nijs, Phys. Rev. Lett. **64**, 435 (1990); in *Phase Transitions in Surface Films 2* (Ref. 7), p. 247.
[16] M. T. Alkhafaji and A. D. Migone, Phys. Rev. B **45**, 8767 (1992); A. D. Migone *et al.*, *ibid.* **47**, 6685 (1993); P. Shrestha and A. D. Migone, *ibid.* **54**, 17 102 (1996).
[17] H. Wu and G. B. Hess, Physica B **194–196**, 965 (1994); Hong Wu, Ph.D. thesis, University of Virginia, 1995.
[18] J. Z. Larese *et al.*, Phys. Rev. B **40**, 4271 (1989).
[19] H. Hong and R. J. Birgeneau, Z. Phys. B **77**, 413 (1989); W. J. Nuttall *et al.*, J. Phys.: Condens. Matter **5**, 8159 (1993).
[20] P. C. Souers, *Hydrogen Properties for Fusion Energy* (University of California Press, Berkeley, 1986).
[21] I. F. Silvera, Rev. Mod. Phys. **52**, 393 (1980).
[22] A. E. Curzon and A. J. Mascall, Br. J. Appl. Phys. **16**, 1301 (1965).
[23] C. Barrett, L. Meyer, and J. Wasserman, J. Chem. Phys. **45**, 834 (1966).
[24] O. Bostanjoglo, Z. Phys. **187**, 444 (1965); O. Bostanjoglo and R. Kleinschmidt, J. Chem. Phys. **46**, 2004 (1967).
[25] J. M. Phillips and C. D. Hruska, Phys. Rev. B **39**, 5425 (1989); J. M. Phillips and N. Shrimpton, *ibid.* **45**, 3730 (1992); J. Z. Larese *et al.*, *ibid.* **37**, 4735 (1988).
[26] J. Ma, D. L. Kingsbury, F. C. Liu, and O. E. Vilches, Phys. Rev. Lett. **61**, 2348 (1988).
[27] A. Pereira, F. Chaves, and E. Lerner, J. Low Temp. Phys. **88**, 421 (1992); L. Diehl, F. Chaves, and E. Lerner, *ibid.* **92**, 173 (1993).
[28] O. E. Vilches *et al.*, in *Excitations in Two-Dimensional and Three-Dimensional Quantum Fluids*, edited by A. G. F. Wyatt and H. J. Lauter (Plenum, New York, 1991), p. 477.

[29] O. E. Vilches, Y-M. Liu, P. S. Ebey, and F.-C. Liu, Physica B **194–196**, 665 (1994).
[30] M. D. Evans and N. S. Sullivan, J. Low Temp. Phys. **100**, 535 (1995).
[31] H. Wiechert, in *Excitations in Two-Dimensional and Three-Dimensional Quantum Fluids*, see (Ref. 28), p. 499.
[32] Wei Liu and S. C. Fain, Jr., Phys. Rev. B **47**, 15 965 (1993).
[33] E.-K. Jeong, B. Ouyang, R. Norberg, P. Fedders, and M. Conradi, Phys. Rev. Lett. **69**, 2983 (1992); M. D. Evans and N. S. Sullivan, J. Low Temp. Phys. **100**, 551 (1995).
[34] P. Zeppenfeld, M. Bienfait, F. C. Liu, O. E. Vilches, and G. Coddens, J. Phys. (France) **51**, 1929 (1990).
[35] M. Maruyama, M. Bienfait, F. C. Liu, Y. M. Liu, O. E. Vilches, and F. Rieutord, Surf. Sci. **283**, 333 (1993).
[36] Y. M. Liu *et al.*, Phys. Rev. B **54**, 6307 (1996); Y. M. Liu, Ph.D. dissertation, University of Washington, Seattle, 1993.
[37] Product of Union Carbide Corp.
[38] T. Takaishi and Y. Sensui, Trans. Faraday Soc. **59**, 2503 (1963).
[39] H. S. Nham and G. B. Hess, Langmuir **5**, 575 (1989).
[40] J. G. Dash, J. Cryst. Growth **100**, 268 (1990).
[41] R. J. Muirhead, J. G. Dash, and J. Krim, Phys. Rev. B **29**, 5074 (1984); D. A. Huse, *ibid.* **29**, 6985 (1984); F. T. Gittes and M. Schick, *ibid.* **30**, 209 (1984).
[42] H. P. Schildberg *et al.*, Jpn. J. Appl. Phys., Suppl. 3, **26**, 343 (1987).
[43] Huse (Ref. 41).
[44] W. F. Saam (private communication).
[45] W. A. Steele, *The Interaction of Gases with Solid Surfaces* (Pergamon, Oxford, 1974), p. 238ff.
[46] S. Chung, N. Holter, and M. W. Cole, Phys. Rev. B **31**, 6660 (1985).
[47] G. Vidali, G. Ihm, H.-Y. Kim, and M. W. Cole, Surf. Sci. Rep. **12**, 133 (1991).
[48] P. B. Weichman and A. Prasad, Phys. Rev. Lett. **76**, 2322 (1996).
[49] H. Mannebach, U. G. Volkmann, J. Faul, and K. Knorr Phys. Rev. Lett. **67**, 1566 (1991).